ARTICLE NO. 78-494

Effects of Purity on Fatigue and Fracture of 7XXX-T76511 Aluminum Extrusion

J. M. Van Orden,* W. E. Krupp,† E. Walden,‡ and J. T. Ryder§
Lockheed-California Company, Burbank, Calif.

The 7050 and 7049 aluminum alloys were developed by Alcoa and Kaiser Aluminum as improvements over the currently used stress corrosion susceptible high-strength 7075-T6 and 7079-T6 compositions, and over the stress corrosion resistant but lower strength 7075-T73. As part of Lockheed's continuing program to correlate fatigue crack growth with fracture toughness, tests were conducted to compare the effects of various impurity levels (iron and silicon) on the plane strain fracture toughness and fatigue crack propagation rates of these alloys. The lower impurity compositions showed significantly higher toughness. Fatigue crack growth rates at stress intensity values below 20 MPa $\sqrt{m}$ (18 ksi $\sqrt{in.}$) showed little variation; however, for stress intensity values greater than 20 MPa $\sqrt{m}$ (18 ksi $\sqrt{in.}$), differences were significant. For example, the crack growth rate for 7075-T76511 at $\Delta K = 30$ MPa $\sqrt{m}$ (27 ksi $\sqrt{in.}$) for the high impurity level was approximately 3.6 times the rate for the low impurity material. Stress corrosion and exfoliation corrosion properties were not affected by the impurity level within the scope of the test. The microstructures and fracture surfaces were examined to correlate differences in fracture and crack growth behavior with constituent particle size and distribution and typical examples are shown in the paper.

Introduction

HIGH-STRENGTH aluminum alloys, such as 7075-T6, offer design advantages over the lower strength alloys by permitting reduction in vehicle weight and increases in performance. The advantages due to higher strength, however, are partially offset by poor stress corrosion and exfoliation corrosion resistance. These factors increase the cost of using the higher strength alloys, because of requirements for corrosion protection, more detailed inspection, more frequent maintenance, and possible service failures. The presence of residual tensile stress promotes stress and exfoliation corrosion. Therefore, residual stresses resulting from heat treatment and assembly must be minimized by limiting heat treatment section sizes, degree of fastener interference fit, and mismatch tolerances. These factors also increase the cost of using these alloys. A partial solution to these problems became available during the 1960s with the development of age-stabilized tempers; for example, 7075-T76 and 7075-T73. The improvements in corrosion resistance, however, were offset by significant reductions in strength, thereby incurring weight penalties.

A more acceptable solution to the problem has been achieved through the recent development of alloys, such as 7049, 7050, and 7475. Improvements in stress corrosion and exfoliation corrosion resistance were achieved with little or no loss in tensile strength.

Along with the development of these new alloy systems, numerous investigators have demonstrated that significant improvements in fracture toughness can be achieved by holding the impurities, i.e., iron and silicon, to very low levels.[1-3] Thompson and Zinkham[4] showed that processing (grain structure and yield strength) and the amount of coarse second-phase particles both affected fracture toughness; however, fatigue crack growth rate did not show any major variations. Therefore, high purity coupled with an optimum distribution of intermediate particles was necessary for high-toughness and low fatigue crack growth rates. Blau[5-7] has reported that iron and silicon had no significant effect on tensile strength or exfoliation corrosion resistance among 20 combinations of composition and processing in 7X75 type alloys, and that varying iron and silicon levels (0.02-0.31%) showed no clear effect on stress corrosion resistance, except when combined with thermomechanical processing (TMP). Recent work by Van Orden and Pettit[8] on 7050-T76511 extrusion has shown that a cleaner microstructure (reflecting better distribution of iron and silicon containing second-phase particles) provided higher fracture toughness; however, no clear difference was noted in fatigue crack growth rate in 3.5% NaCl.

The referenced work (performed on extrusion, sheet, plate, and forging products) shows that lower impurity (iron, silicon) levels will provide significant improvements in fracture toughness. However, unless additional processing is also utilized, no clear improvements are realized in fatigue crack growth rates.

The purpose of the work reported here was to determine the effects of the impurity level (i.e., iron and silicon) on several critical properties, especially plane strain fracture toughness and plane strain fatigue crack growth rate in a corrosive environment. Alloys tested were fabricated under identical conditions with no additional special mill processing, i.e., in a commercially available product form. The intent was to isolate the effects of impurities from the many other factors that can have interrelated effects on the properties of primary interest.

Test Materials and Test Specimens

The test materials used in this program (7049, 7075, and 7050 aluminum alloy extruded bars) were prepared from seven 229 mm (9 in.) diam ingots, which were converted, utilizing best commercial practice, by extruding at 427°C (800°F) with an extrusion reduction ratio of 10, to 38 × 114 mm (1.5 × 4.5 in.) bars. The bars were solution heat-treated at 460°C (860°F), stress relieved by stretching, then aged at 121°C (250°F) for 24 h followed by second-step aging at

Presented as Paper 78-494 at the AIAA/ASME 19th Structures, Structural Dynamics and Materials Conference, Bethesda, Md., April 3-5, 1978; Submitted May 19, 1978; revision received Nov. 2, 1978.

Index categories: Structural Materials; Structural Durability (including Fatigue and Fracture); Materials, Properties of.

*Research Scientist, Engineering Laboratories Division. Member AIAA.
†Group Engineer, Engineering Laboratories Division.
‡Research Specialist, Engineering Laboratories Division.
§Research Scientist, Engineering Laboratories Division.

163°C (325°F) for 10, 14, or 17 h (7049, 7075, and 7050, respectively) to provide the -T76511 condition. These aging conditions were selected intentionally to provide materials with comparable mechanical properties.

The -T76511 condition is an intermediate strength condition between the highest (-T6) and lowest (-T73) strength conditions used extensively by Lockheed to provide an optimum strength/corrosion resistant combination of properties for the 7075 alloy. It also has been successfully applied to the 7049 and 7050 alloys for the same reasons.

The chemical compositions for the materials are listed in Table 1 along with the published compositions for the alloys. The 7049 and 7075 were prepared with three levels of iron and silicon, and the 7050 was prepared with only the low-impurity composition currently specified for this alloy. The impurity levels for the 7049 and 7075 were held within the specification ranges; the other elements were held to commercial nominal values. No attempt was made to alter constituent, dispersoid, or precipitate particle size or distribution, e.g., with special thermomechanical processing, heat treatment, etc., of the test bars. The low-impurity 7075 material composition is essentially equivalent to the 7475 alloy developed by the Aluminum Company of America, without the proprietary processing associated with that alloy. In addition to the standard mechanical property test specimens, fatigue, fracture toughness, fatigue crack growth, stress corrosion, and exfoliation corrosion test specimens were prepared. Fatigue test specimens were machined round with a circumferential notch to provide a stress concentration factor $K_t = 3$. Fracture toughness and fatigue crack growth specimens were prepared in accordance with the ASTM E399 compact specimen with $B = 19$ or 31.8 mm (0.75 or 1.25 in.) $= W/2$ and $W/4$, respectively ($W/4$ for the crack growth specimens only). Stress corrosion test specimens were machined as small tensile specimens 31.8 mm (1.25 in.) long with a 3.2 mm (0.125 in.) diam and a 12.7 mm (0.5 in.) long test section in accordance with ASTM G47-76. Stepped exfoliation corrosion test coupons were machined to expose the T/10 plane and T/2 or midplane of the extrusion. All of the test specimens were machined from the middle plane of the extruded bars.

Tensile test specimens were prepared in all three grain directions—longitudinal (L) (parallel to the direction of major working), transverse (T) (perpendicular to the direction of major working), and short transverse (S) (through the thickness). Fatigue and exfoliation corrosion specimens were prepared in the L direction only. Duplicate fracture toughness and single fatigue crack growth specimens were prepared in the LT (L is the loading direction and T is the direction of crack growth) and TL orientations. Stress corrosion specimens were prepared in the S direction only.

Testing

The tensile tests were conducted in accordance with ASTM E8 procedures. Constant amplitude fatigue tests were conducted in accordance with the procedures established in ASTM STP No. 91 entitled, "Manual on Fatigue Testing." The tests were performed in resonant machines at a load application frequency of approximately 1800 cycles/min. A stress ratio (R) of +0.1 was used and the maximum stress levels applied to the specimens were varied to define the S-N curve from approximately 10^4-10^7 cycles. The fatigue data were then compared with reference data. Fracture toughness tests were conducted in accordance with the procedures outlined in ASTM E399-72, utilizing the compact specimen with $B = 19$ or 31.8 mm (0.75 or 1.25 in.) $= 0.5$ W. Fatigue crack propagation tests were conducted under plane-strain stress intensity conditions. The specimens were fatigue precracked in air at $R = +0.1$ and 6 Hz to a length of approximately 2.54 mm (0.10 in.). Decreasing loads were used during precracking so that the final 0.5 mm (0.02 in.) increment of crack length was generated at a stress intensity equal to the initial test stress intensity. After precracking, the test specimens were dried at 150°F for 10 min before the environmental chamber was placed around the specimen. Tests were conducted in 3.5% sodium chloride solution.

Crack growth tests were conducted beginning with an initial load equal to the final precracking load and then with incrementally increased loads until final fracture. A range ratio of +0.1 and a frequency of 6 Hz were used for the entire test. Crack growth was measured optically and recorded at 0.38-0.5 mm (0.015-0.020 in.) growth increments. All tests were performed in servocontrolled electrohydraulic fatigue machines with peak and valley load monitoring, such that maximum and minimum load per cycle was controlled within ±1% of maximum load.

The cyclic test load vs crack length data were converted into crack growth rate (da/dN) vs stress intensity factor (ΔK), according to established practice. The stress intensity factor (ΔK value), corresponding to each measured increment of crack growth, is computed on the basis of the average crack length in the interval $(a_i + a_{i+1})/2$ and the varying component of fatigue stress, which is a function of the load and given by the formula $\Delta P = (1 - R)P$. The formulation for ΔK is otherwise identical to that for K as given in ASTM E399-72. The tests were limited to the range $0.45 \leq a/W \leq 0.7$. The crack growth rate during each increment is approximated by the relation $(a_{i+1} - a_i)/(N_{i+1} - N_i)$. The results, in the form of da/dN vs ΔK, were plotted automatically using a Calcomp plotter.

The data were processed for presentation in a graphical format so the plotted data could be shown along with the 2σ curve-fit scatter bands for test specimen sets. The crack

Table 1 7XXX alloy compositions

Alloy type	Impurity level	Elements, %										
		Si	Fe	Cu	Mn	Mg	Cr	Ni	Zn	Ti	Pb	Zr
7049	Low	0.08	0.09	1.50	0.01	2.49	0.21	0.00	7.75	0.01	0.04	0.00
7049	Medium	0.11	0.20	1.60	0.01	2.35	0.20	0.00	7.92	0.01	0.04	0.00
7049	High	0.16	0.37	1.60	0.02	2.31	0.19	0.00	7.80	0.01	0.04	0.00
7075[a]	Low	0.08	0.11	1.40	0.01	2.40	0.20	0.00	6.05	0.01	0.00	0.00
7075	Medium	0.13	0.21	1.45	0.01	2.41	0.20	0.00	5.85	0.01	0.03	0.01
7075	High	0.17	0.33	1.60	0.02	2.40	0.20	0.01	6.00	0.01	0.03	0.00
7050	Low	0.05	0.10	2.30	0.01	2.40	0.03	0.01	6.35	0.01	0.02	0.12
7049[b]		0.25	0.35	1.2-2.9	0.20	2.0-2.9	0.10-0.22	-	7.2-8.2	0.10	-	-
7075[b]		0.40	0.50	1.2-2.0	0.30	2.1-2.9	0.18-0.35	-	5.1-6.1	0.20	-	-
7050[b]		0.12	0.15	2.0-2.6	0.10	1.9-2.6	0.04	-	5.7-6.7	0.06	-	0.08-0.15

[a] This composition is similar to the 7475 alloy developed by Alcoa, but without the proprietary processing associated with this alloy. [b] Aluminum Association—Percent maximum unless shown as a range.

growth data taken at one test set were combined and empirically fit using the following expression used by Ryder,[9] which is based on the form of the Gumbel double-exponential distribution

$$da/dN = \text{Exp}\{u - \ell n[-\ell n(1-\Delta K/K_d)]/\alpha\} - 1 \quad (1)$$

where α and u are constants for a particular data set and K_d, also a constant for a particular data set, is the $K_{max.}$ value at fracture of a crack growth coupon.

Equation (1) is based on several related investigations at Lockheed-California Company into curve-fitting algorithms, which were inspired by Bowie and Sandifer[10] and reduced to practice by Ryder.[9] For completeness, one should be aware that Eq. (1) has the advantage that the stress intensity at which the crack growth rate rapidly decreases, K_{th}, is determined by the data rather than arbitrarily chosen. For the final value of K_d selected, the threshold stress intensity can be extrapolated as:

$$K_{th} = K_d\{1 - \text{Exp}[-\text{Exp}(\alpha u)]\} \quad (2)$$

In keeping with practice established when crack growth data trends were approximated by means of hand drawn curves, the stress intensity range at the transition from slow to fast growth (ΔK_{sf}) was determined by calculating the ΔK value at the minimum value of the risk function (r), which is defined as:

$$r = \frac{d\ell n(da/dN)}{d\Delta K} = \frac{1}{da/dN}\frac{d(da/dN)}{d\Delta K} \quad (3)$$

The stress intensity range parameter ΔK_{sf} is effectively the highest ΔK at which a crack can be said to be in slow propagation. Beyond ΔK_{sf}, no usable fatigue crack life remains, except in a low-cycle fatigue case, due to high growth rates. The advantage of calculating ΔK_{sf} is in precisely defining the ΔK value above which the life of the component is in the low-cycle fatigue regime.

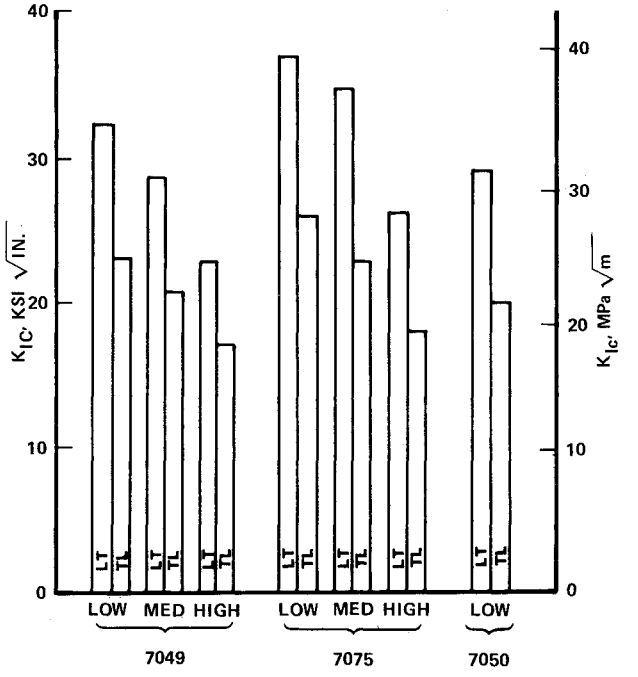

Fig. 1 Results of fracture toughness tests on 7XXX-T76511 extruded bar with low, medium, and high impurity levels.

Based on Eq. (1), a median crack growth curve was defined as that corresponding to the α and u values found by linear regression. The 2σ limit scatter bands were found by substituting $u = -(\alpha \pm 2\sigma)/b$ into Eq. (1). A curve which can be used as a useful design curve to give a conservative life estimate was defined by substituting $u = -(\alpha - \sigma)/b$ into Eq. (1), which resulted in a left-side 1σ scatter band curve. Figure 11 shows typical 2σ scatter bands and a suggested design curve for one of the test specimens.

Stress corrosion test specimens were axially loaded in test fixtures to two stress levels and exposed to alternate immersion (10 min immersed, 50 min dry per cycle) in a 3.5% sodium chloride-water solution for a period of 30 days and inspected daily for failures. The alternate immersion test procedure is described in MIL-H-6088D and the stress corrosion test was conducted per ASTM G47-76.

The exfoliation corrosion test specimens were subjected to three environmental tests:

1) ASTM G34-72 (EXCO) test, 48 h.

2) Alternate salt spray test [7 days (28 cycles) – 5% NaCl, pH 3.0-3.1, 45 min spray, 2 h force dry, 3-1/4 h at 100% relative humidity].

3) Sea coast air exposure at Pt. Loma, Calif. for 2 years.

Test specimens were photographed after the exposures and then metallurgically examined to determine the type of corrosion.

Results

Static Tests

The results of the static mechanical properties tests indicated only slight decreases in tensile properties and ductility with increasing impurity level in the 7049-T76511 and 7075-T76511. Only one (low impurity) lot of 7050-T76511 was tested.

Fatigue Tests

Comparative constant amplitude fatigue test data for the 7049-T76511 extruded bar and 7050-T76511 extruded shape from an earlier test program[8] showed little differences between the 7049 and 7050 test data and little differences among the 7049 lots with varying impurity contents.

Fracture Toughness Tests

The results of the fracture toughness tests are presented in Fig. 1. The test showed that specimen thickness (B) was a significant factor. The results for 31.8-mm (1.25-in.) thick specimens were generally lower than those for 19-mm (0.75-in.) thick specimens. The data for the thicker specimens (Fig. 1) were found to be valid when tested in accordance with the ASTM E399 test for validity.

The data show a significant increase in toughness with decreasing level of iron and silicon. For example, the toughness for 7075-T76511 in the longitudinal orientation with low impurity level was 40.7 MPa $\sqrt{m}$ (37 ksi $\sqrt{in.}$) and for high impurity material it was 30% lower. The 7049-T76511 results were similar. The results also showed that the longitudinal (LT) specimens showed higher fracture toughness than the transverse (TL) specimens.

The lower fracture toughness values for specimens in the TL orientation were attributed in large part to the presence of the (iron-rich) second-phase particles lying along the grain boundaries. In the LT orientation, the crack front proceeds across the grains and grain boundaries and, therefore, is less affected by the presence of the inclusions. These findings are supported by the significant decreases in fracture toughness with increasing iron and silicon content. Typical test specimens were sectioned to show this and the results are presented in Figs. 2-4.

Scanning electron microscope fractographs of typical fracture surfaces are presented in Figs. 5 and 6. The increasing size of the microvoids and second-phase particles (many of

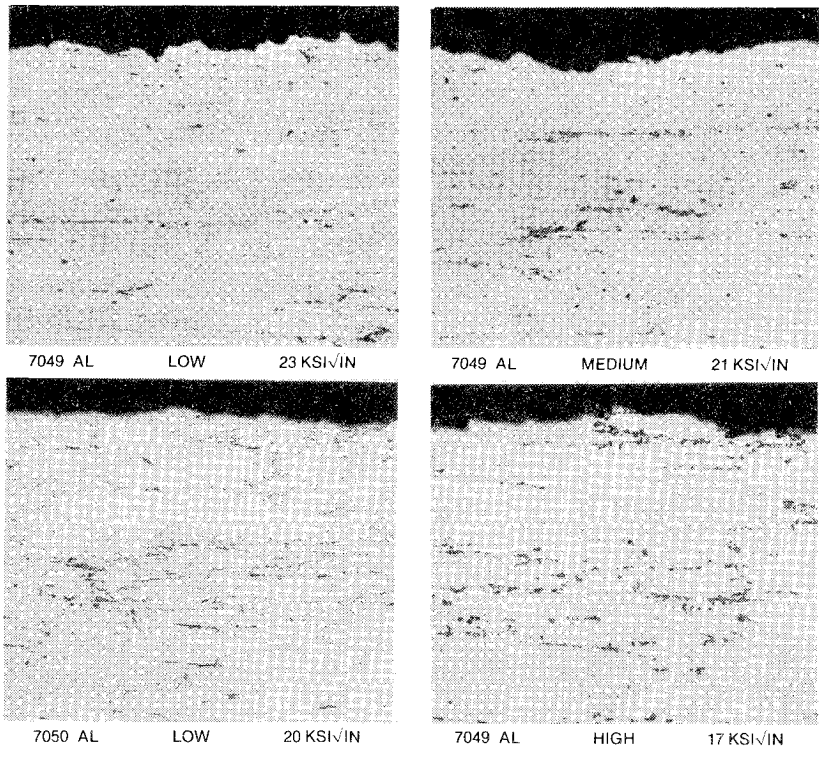

Fig. 2 Profiles of 7049-T76511 and 7050-T76511 fracture toughness specimens (*TL*) illustrating comparative inclusion contents. The fracture is along the upper edge in the photos. Magnification: 50X.

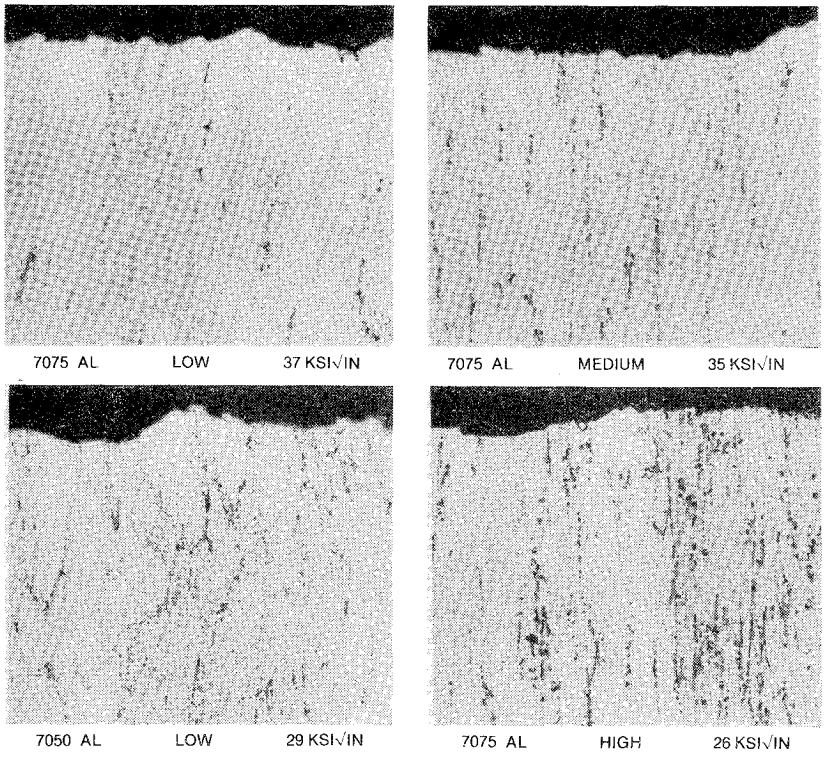

Fig. 3 Profiles of 7075-T76511 and 7050-T76511 fracture toughness specimens (*LT*) illustrating comparative inclusion contents. The fracture is along the upper edge in the photos. Magnification: 50X.

which are cracked or fractured) with increasing iron and silicon content is evident in the photographs of the overload or fast-fracture portions of the fracture surfaces. These photographs also show that the fatigue precracking areas of the fracture surfaces are comparatively free of the second-phase particles, i.e., the fatigue crack growth at the low stress intensities used for precracking of the fracture toughness specimens is virtually unaffected by the presence of the second-phase particles. This observation is supported further in the following discussion of the fatigue crack growth rate test results.

The results of the fracture toughness test presented here may help to explain the relatively large amount of scatter in published toughness data for aluminum alloys with compositions that are within the specified ranges for commercial products, but vary in iron and silicon content.

Fatigue Crack Growth Rate Tests

The fatigue crack growth rate data are plotted in Figs. 7-9 for the 7049-T76511, 7075-T76511, and 7050-T76511, respectively. All of the data for each of the alloys in both grain directions and several impurity levels are plotted

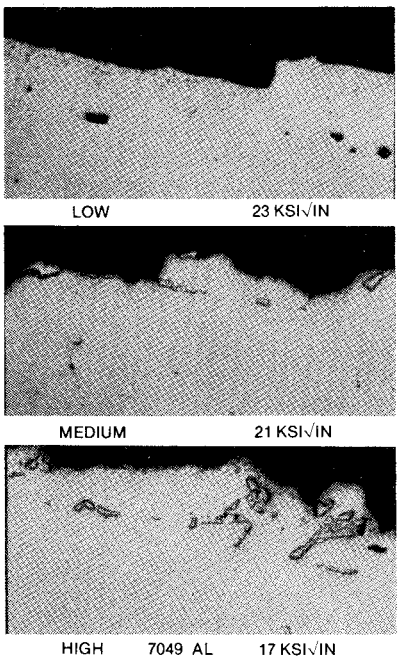

Fig. 4 Profiles of 7049-T76511 fracture toughness specimens illustrating inclusions lying along the fracture. Impurity levels are as indicated. Magnification: 250X.

together in each of the figures; the data for all three alloys are plotted in Fig. 10. In general, for stress intensity values below 20 MPa $\sqrt{m}$ (18 ksi $\sqrt{in.}$) crack growth rates showed little difference between the two grain directions (*LT* and *TL*) and among the three impurity levels tested for the 7049-T76511 and 7075-T76511 (only one lot of 7050-T76511 was tested).

For stress intensity values greater than 20 MPa $\sqrt{m}$ (18 ksi $\sqrt{in.}$), some differences were apparent. For example, the specimens oriented in the *TL* direction failed at values near 20 MPa $\sqrt{m}$ (18 ksi $\sqrt{in.}$) in all three alloys and impurity levels. Additionally, the high-purity specimens in the *LT* orientation showed lower crack growth rates at stress intensities greater than 20 MPa $\sqrt{m}$ (18 ksi $\sqrt{in.}$) in the 7049-T76511 and 7075-T76511. For example, the crack growth rates for 7075-T76511 with high and low impurity levels were 2.0×10^{-5} m/cycle (7.8×10^{-4} in./cycle) and 5.5×10^{-6} m/cycle (2.1×10^{-4} in./cycle), respectively, at $\Delta K = 30$ MPa $\sqrt{m}$ (27 ksi $\sqrt{in.}$). The rate for the high impurity level is approximately 3.6 times the rate for the low impurity material. Other similar comparisons can be made for other compositions and stress intensities.

The overall comparison of plotted crack growth rate data for the three alloys, two grain directions, and three impurity levels (Fig. 10) indicates no easily discernible differences among the various test materials and grain directions. Accordingly, the data for each test set were fitted to a curve using the equations; data points for each individual specimen were then superimposed on a general 2σ curve band of all the data for each set of alloy/orientation/impurity levels to illustrate more clearly any differences in the data plots. Typical results are presented in Figs. 11-14 for the 7075-T76511.

Close examination of the data points superimposed on the 2σ bands in Figs. 11, 13, and 14 for 7075-T76511 reveals a general increase in crack growth rates in the *LT* grain orientation with increasing impurity levels toward the left 2σ curve (higher crack growth rates for the same stress intensity), at stress intensities above 20 MPa $\sqrt{m}$ (18 ksi $\sqrt{in.}$). Data for the *TL* orientation showed less scatter (typical curves are shown in Fig. 12), higher crack growth rates, and failure at

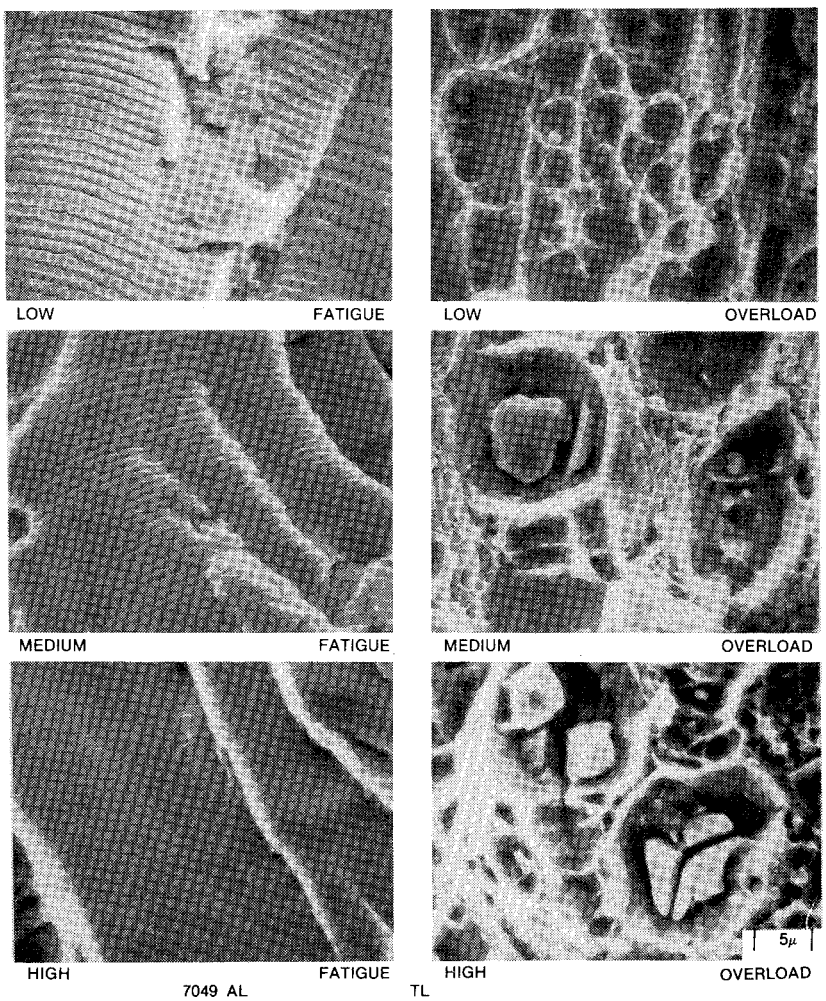

Fig. 5 Scanning electron microscope fractographs of fracture toughness specimens illustrating the precracking (fatigue) and fast fracture (overload) areas. Note the inclusion and microvoid sizes. Orientation—*TL*. Magnification: 1500X.

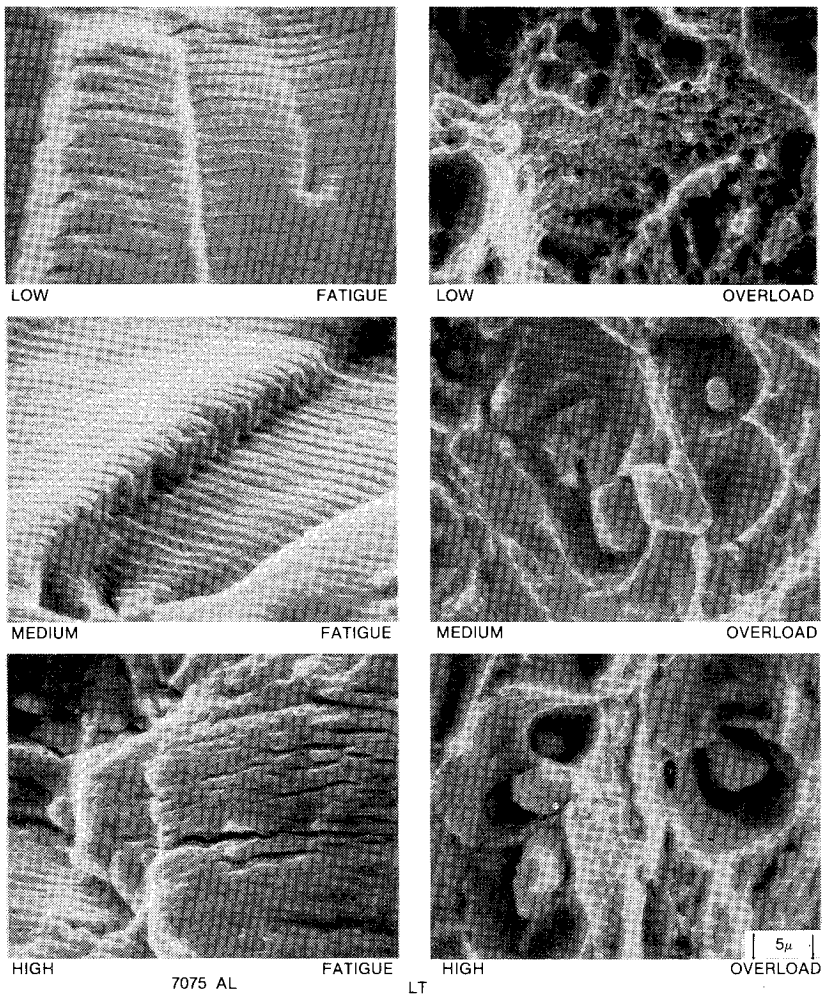

Fig. 6 Scanning electron microscope fractographs of fracture toughness specimens illustrating the precracking (fatigue) and fast fracture (overload) areas. Note the inclusion and microvoid sizes. Orientation—*LT*. Magnification: 1500X.

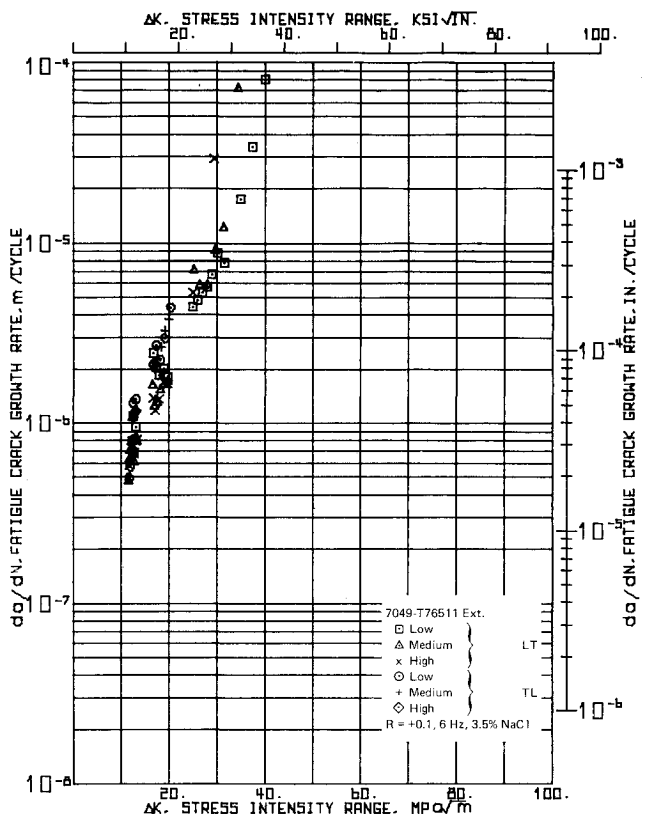

Fig. 7 Fatigue crack growth rates for 7049-T76511 extrusions with various impurity levels (low, medium, high) and two grain directions (*LT, TL*).

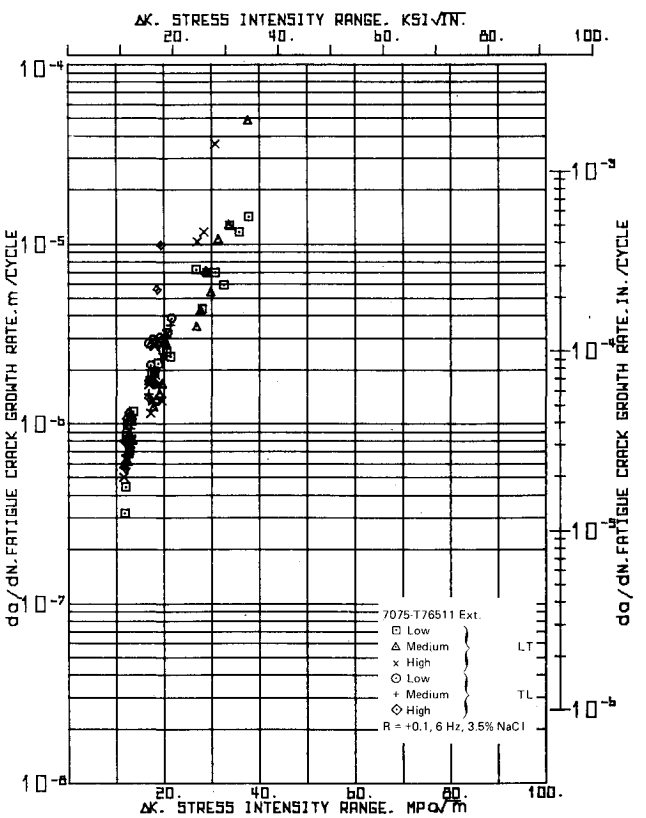

Fig. 8 Fatigue crack growth rates for 7075-T76511 extrusions with various impurity levels (low, medium, high) and two grain directions (*LT, TL*).

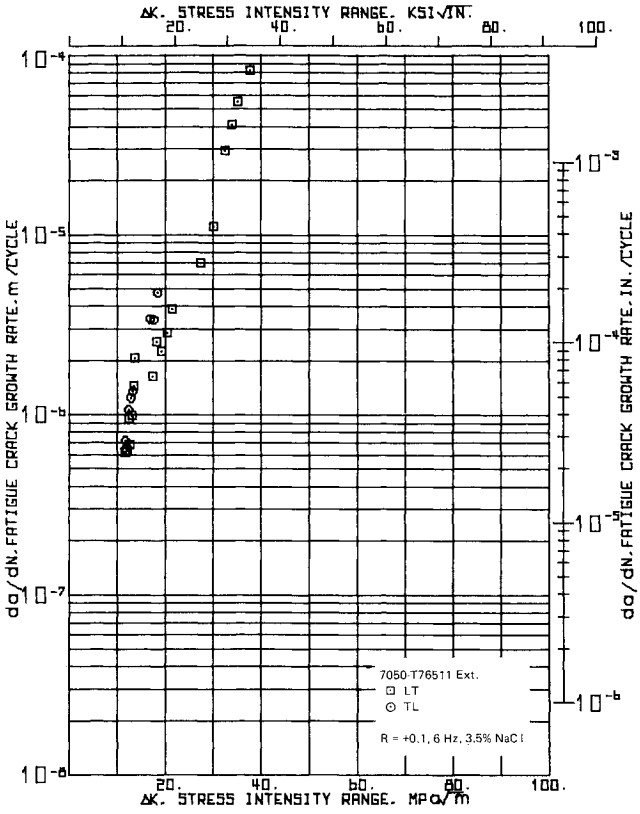

Fig. 9 Fatigue crack growth rates for 7050-T76511 extrusion with low impurity level in two grain directions (*LT, TL*).

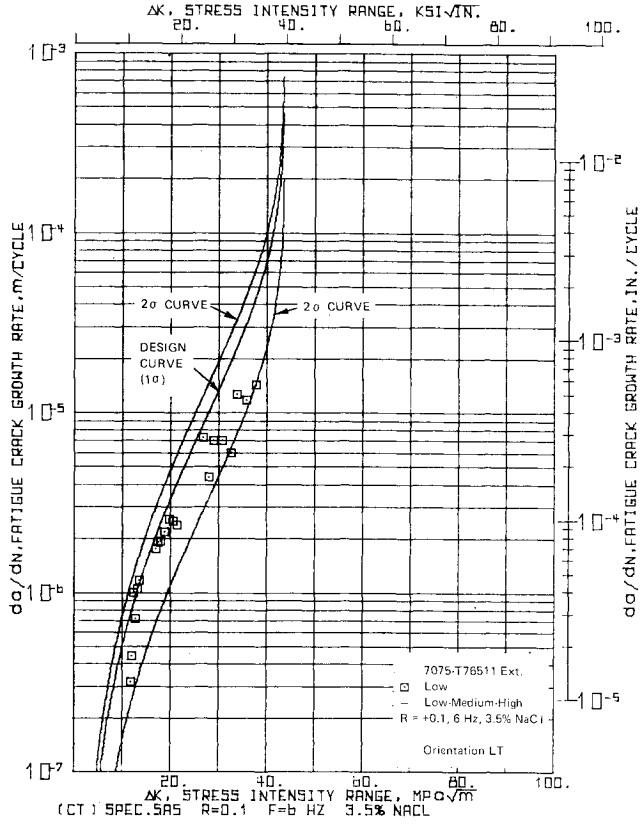

Fig. 11 Fatigue crack growth rate for low impurity 7075 aluminum alloy extrusion. Solid lines are 2σ curves and the design curve (1σ) for the three impurity levels of this material.

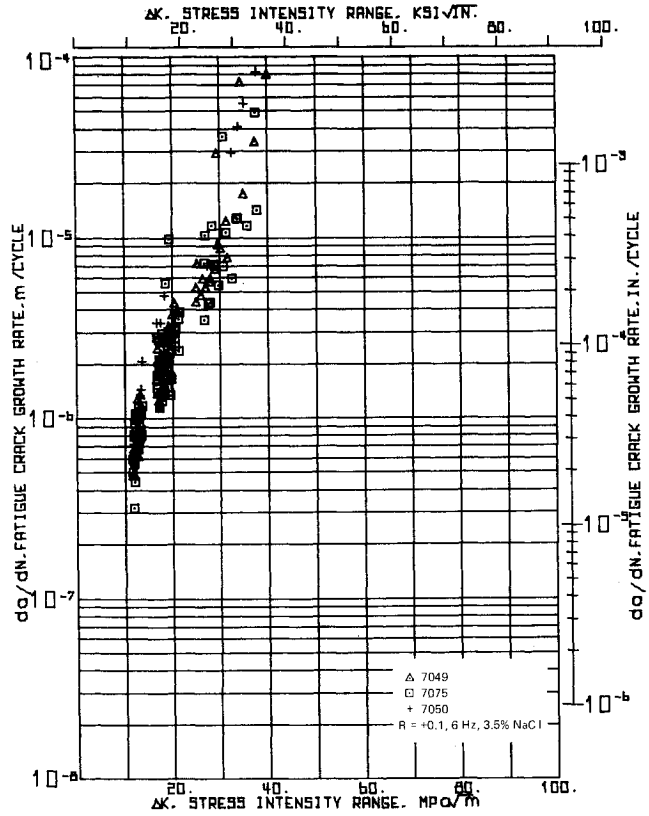

Fig. 10 Comparative fatigue crack growth rates for 7XXX-T76511 extrusions.

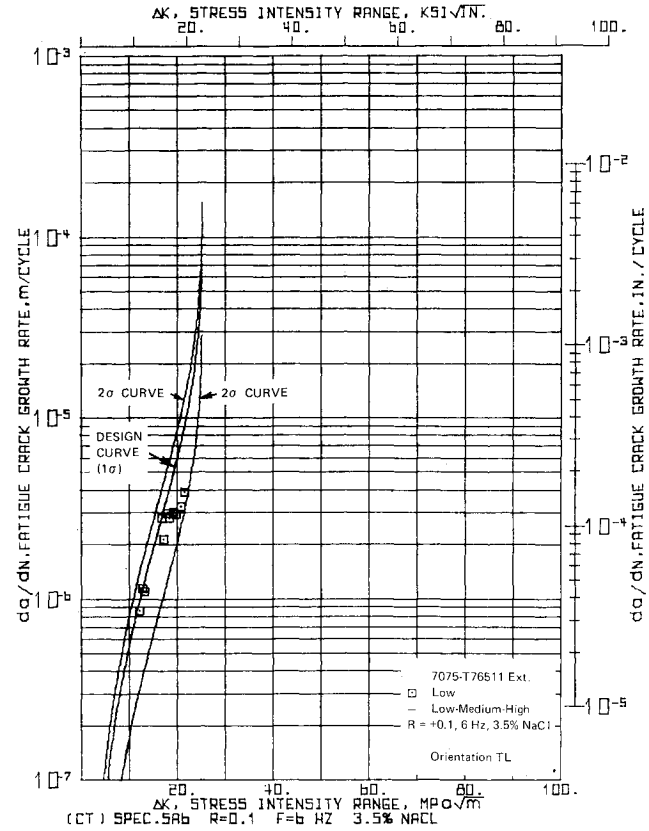

Fig. 12 Fatigue crack growth rate for low impurity 7075 aluminum alloy extrusion.

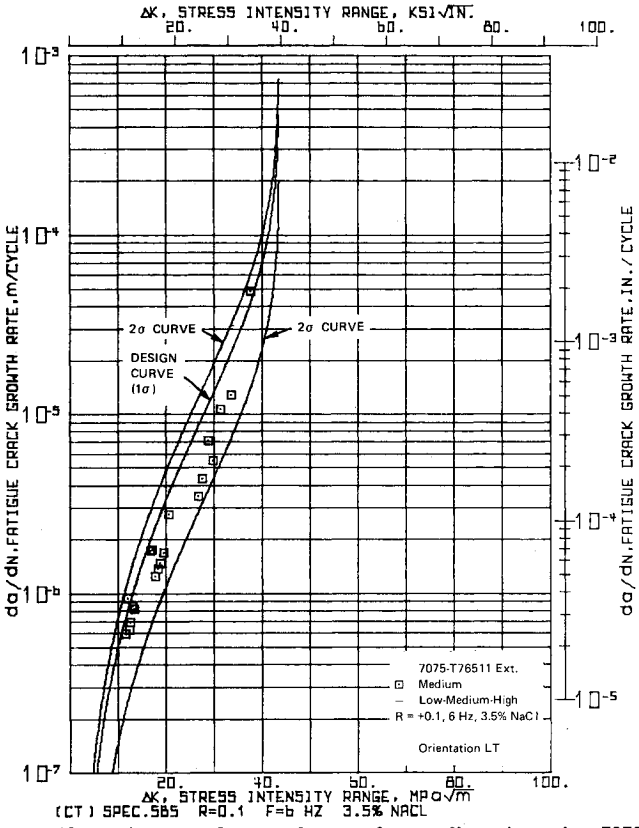

Fig. 13 Fatigue crack growth rate for medium impurity 7075 aluminum alloy extrusion.

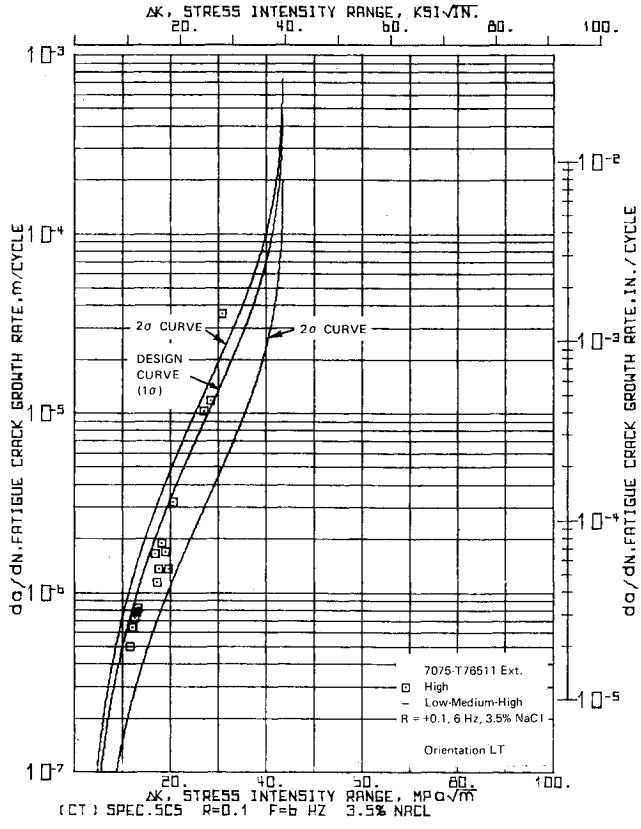

Fig. 14 Fatigue crack growth rate for high impurity 7075 aluminum alloy extrusion.

lower stress intensities (reflecting lower K_{Ic} for this orientation). Similar trends were noted for the 7049-T76511.

The test results showed that the fatigue crack growth rates in 3.5% salt water were virtually unaffected by increasing iron and silicon content at the lower stress intensities [<20 MPa $\sqrt{m}$ (18 ksi $\sqrt{in.}$)]. This was demonstrated also in the discussion on fracture toughness earlier in the paper. At the higher stress intensities (>20 MPa $\sqrt{m}$), i.e., in the higher crack growth rate regions, the increasing iron and silicon caused increased crack growth rates. Since the higher growth rates would be associated with shorter life (i.e., the low cycle or limited fatigue life range), the lower growth rate region is of primary interest in life prediction analyses.

Thus, the test has demonstrated that impurity content may not be a significant factor in plane strain fatigue crack growth rate in the crack growth region of design interest, in spite of the very significant improvements in fracture toughness in the cleaner materials. This finding should be assessed also on these materials when tested under plane stress conditions, i.e., on thin plate and sheet products.

The results of the tests probably reflect the scatter that can be expected with material containing varying amounts of impurities within the specified composition ranges for each alloy system.

A summary of the analysis of all the crack growth data, utilizing the procedure developed by Ryder[9], is presented in Table 2, which shows the threshold stress intensity (ΔK_{th}), the stress intensity at which the slow to fast crack growth rate transition occurs (ΔK_{sf}), and the ratio of ΔK_{sf} to K_d, all based on the design (1σ) curve. The results show that the ΔK_{th} values are all similar, in spite of the significant differences in fracture toughness among the specimens. The values of ΔK_{th} which were computed (Table 2) appear to be relatively lower than the values indicated on the crack growth curves, i.e., where the curves intersect the stress intensity lines. This can be explained by close inspection of these ends of the curves in that they are still sloping toward the left, and they would eventually intersect at a lower value of stress intensity at a lower crack growth rate than that indicated on the curves. The ΔK_{sf} values were quite similar for all of the materials and impurities for given grain directions (Table 2), except for the 7049-T76511 low-impurity material in the LT grain direction. At a crack growth rate da/dN of 1×10^{-6} m/cycle (3.9×10^{-5} in./cycle), the stress intensities were essentially equivalent for all of the materials, impurity levels, and grain directions tested (Table 2).

Stress Corrosion Tests

The stress corrosion tests on the 7049-T76511 showed that impurity levels within the specified composition range did not affect stress corrosion resistance at stresses up to 241 MPa (35 ksi). The other alloys were not tested; however, it is expected that the results would have been similar. Although general pitting corrosion increased in severity with increasing impurity level, the criteria indicating stress corrosion susceptibility in the ASTM G47-76 procedure, i.e.,-failure during the test or evidence of intergranular attack were not in evidence.

Exfoliation Corrosion Tests

The results of the exfoliation corrosion tests indicated no significant differences for the three impurity levels tested in the 7049-T76511 in the 48-h EXCO test, the 7-day salt spray test, or after 2 years of exposure at the Pt. Loma, Calif. sea coast exposure test site. The other two alloys were not tested; however, it is expected that the results would have been similar. Pitting corrosion was observed on the EXCO and salt spray test specimens, and only mild gray weathering was observed on the specimens exposed at Pt. Loma; the exposure will be continued for several more years. Thus, a criterion for susceptibility to exfoliation corrosion, i.e., leafing, intergranular attack, or delamination in the ASTM G34-72 procedure, was not in evidence on these specimens.

Table 2 Specimen identity and numerical analysis summary

(Range ratio = +0.1, frequency = 6 Hz, environment – 3½% NaCl) (7XXX-T76511 aluminum alloy extruded bar)

Specimen[a]	Impurity level[b]	Alloy (orientation)	K_d MPa$\sqrt{m}$	K_d (ksi$\sqrt{in.}$)	ΔK_{th}[c] MPa$\sqrt{m}$ (ksi$\sqrt{in.}$) (extrapolated)		Risk function (r)	ΔK_{sf}[d] MPa$\sqrt{m}$	ΔK_{sf}[d] (ksi$\sqrt{in.}$)	$\Delta K_{sf}/K_d$	ΔK[e] (da/dN at 10^{-6} m/cyc) MPa$\sqrt{m}$	ΔK[e] (da/dN at 10^{-6} m/cyc) ksi$\sqrt{in.}$
9A5	Low	7049 (LT)	45.7	(41.5)	2.78	(2.53)	0.1322	28.9	(26.3)	0.634	13	11.8
9B5	Medium	7049 (LT)	40.7	(37.0)	3.91	(3.55)	0.1777	25.8	(23.5)	0.634	14	12.7
9C5	High	7049 (LT)	31.9	(29.0)	3.19	(2.90)	0.1871	20.3	(18.5)	0.638	15	13.6
9A6	Low	7049 (TL)	20.9	(19.0)	1.25	(1.16)	0.1887	13.4	(12.2)	0.642	13	11.8
9B6	Medium	7049 (TL)	20.9	(19.0)	0.77	(0.70)	0.1558	13.4	(12.2)	0.641	13	11.8
9C6	High	7049 (TL)	14.3	(13.0)	2.18	(1.98)	0.2854	9.6	(8.7)	0.669	13	11.8
5A5	Low	7075 (LT)	43.6	(39.6)	2.00	(1.82)	0.1157	27.7	(25.2)	0.635	13	11.8
5B5	Medium	7075 (LT)	43.6	(39.6)	2.71	(2.46)	0.1323	27.7	(25.2)	0.634	14	12.7
5C5	High	7075 (LT)	43.6	(39.6)	4.22	(3.84)	0.1779	27.6	(25.1)	0.634	15	13.6
5A6	Low	7075 (TL)	27.5	(25.0)	1.46	(1.33)	0.1595	17.5	(15.9)	0.638	12	10.9
5B6	Medium	7075 (TL)	25.5	(23.2)	1.42	(1.29)	0.1597	16.3	(14.8)	0.640	13	11.8
5C6	High	7075 (TL)	27.5	(25.0)	4.82	(4.38)	0.3238	17.5	(15.9)	0.637	13	11.8
05	Low	7050 (LT)	50.3	(45.7)	3.47	(3.20)	0.1479	31.8	(28.9)	0.633	13	11.8
06	Low	7050 (TL)	21.9	(19.9)	2.50	(2.27)	0.2495	14.1	(12.8)	0.643	12	10.9

[a] Test specimen per ASTME399 CT B = 19 mm (0.75 in.) = W/4. [b] Fe and Si content (see Table 1). [c] Extrapolated threshold ΔK based on 1σ design curve. [d] ΔK at slow to fast crack growth. [e] Values taken from graphs.

Synopsis

The results of this test program have shown that variations in the amounts of impurities (i.e., iron, silicon) within the specification limits for several 7XXX series aluminum alloys can produce significant effects on the fracture toughness and fatigue crack propagation rates in a corrosive environment. The effects on crack growth rates are mixed, depending upon the crack growth rate/stress intensity region of interest to the materials engineer. Mechanical properties, constant amplitude fatigue, and corrosion resistance properties are not shown to be affected significantly by the impurities. Thus, where fracture toughness is a critical design property, limiting of impurities to low levels can be considered cost effective. Where fatigue crack growth resistance is important, little benefit is derived in the more important low stress-low growth rate region [$\Delta K < 20$ MPa $\sqrt{m}$ (18 ksi $\sqrt{in.}$)]. The added costs incurred by imposing severe limits on the amounts of impurities in these high-strength structural alloys may be of marginal benefit depending upon the combination of properties required for a particular design.

Acknowledgments

The authors are indebted to many people at Lockheed-California Company, the Air Force Materials Laboratory, Dayton, Ohio, and Martin Marietta Aluminum Company, Torrance, Calif., and their contributions in the planning, preparation of test materials, testing, discussions, and analysis phases are gratefully acknowledged. Special recognition is accorded J. H. Wooley, G. G. Wald, S. Krystkowiak, W. Fitze, F. Pickel, C. Looper, L. Reed, R. Brodie, Dr. G. Bowie, and W. Budd, all of the Lockheed-California Company; P. J. Blau, R. Geisendorfer and C. L. Harmsworth of the Air Force Materials Laboratory, Wright-Patterson Air Force Base, Ohio; and W. C. Rotsell and D. Mellem, Martin Marietta Aluminum Company, Torrance, Calif.

References

[1] Peel, C.J., Wilson, R.N., and Forsyth, P.J.E., "Relationships Between Some Microstructural Features and the Fracture Toughness of an Al-Zn-Mg-Cu-Mn Forging Alloy," *Metal Science Journal*, Vol. 6, 1972. pp. 102-106.

[2] Quist, W.E. and Hyatt, M.V., "The Effect of Chemical Composition on the Fracture Properties of Al-Zn-Mg-Cu Alloys," Boeing Company, Seattle, Wash. AIAA Paper A66-28009, Cocoa Beach, Fla., April 1966.

[3] Hahn, G.T. and Rosenfield, A.R., "Metallurgical Factors Affecting Fracture Toughness of Aluminum Alloys," *Metallurgical Transactions A*, Vol. 6A, April 1975, pp. 653-670.

[4] Thompson, D.S. and Zinkham, R.E., "The Effects of Alloying and Processing on the Fracture Characteristics of Aluminum Sheet," *Engineering Fracture Mechanics*, Vol. 7, Pergamon Press, New York, 1975, pp. 389-409.

[5] Blau, P.J., "Effects of Purity and Processing on the Exfoliation Corrosion Behavior of 7X75 Aluminum Plate," AFML-TR-75-43, July 1975.

[6] Blau, P.J., "Effects of Iron and Silicon Content on Stress Corrosion Cracking in a Thermomechanically Processed Aluminum Alloy," AFML-TR-75-215, March 1976.

[7] Blau, P.J., "Influence of Iron and Silicon Content on the Tensile Properties of 7X75 and Zr-Modified 7X75 Aluminum Plate," AFML-TR-75-140, Oct. 1975.

[8] Van Orden, J.M. and Pettit, D.E., "Corrosion Fatigue Crack Growth in 7050 Aluminum Alloy Extrusions," Presented as Paper 75-806 at the AIAA 16th Structures and Materials Conference, May 1975; also published in the *Journal of Aircraft*, Vol. 10, Nov. 1976, pp. 873-879.

[9] Ryder, J.T., "Fracture Control of H-O Engine Components," NASA CR-135137, Contract No. NAS3-18896, Final Rept., Feb. 1977.

[10] Sandifer, J.P. and Bowie, G.E., "Double Exponential Functions That Describe Crack Growth Rate Behavior," AIAA Paper 77-763, San Diego, Calif., March 1977.